CMS Physics Analysis Summary

Contact: cms-pag-conveners-exotica@cern.ch 2011/07/21

Search for Stopped Heavy Stable Charged Particles in pp collisions at $\sqrt{s} = 7$ TeV

The CMS Collaboration

Abstract

We present the updated results of a search for long-lived particles which have stopped in the Compact Muon Solenoid detector after being produced in 7 TeV pp collisions from CERN's Large Hadron Collider. We looked for the subsequent decay of these particles during time intervals where there were no pp collisions in the Compact Muon Solenoid experiment. In particular, we searched for decays during gaps between crossings in the Large Hadron Collider beam structure. We recorded such decays with a dedicated calorimeter trigger. In a dataset that is sensitive to an integrated luminosity of up to 886 pb^{-1}, depending on the particle lifetime, and a search interval corresponding to 168 hours of LHC operation, no significant excess above background was observed. In the absence of a signal, we set limits at 95% C.L. on gluino and stop production over 13 orders of magnitude of particle lifetime.

1 Introduction

Many extensions of the standard model predict the existence of new Heavy quasi-Stable Charged Particles [1] (HSCP). Such particles are present in some supersymmetric models [2–4], "hidden valley" scenarios [5], and grand-unified theories (GUTs), where the new particles decay through dimension five or six operators suppressed by the GUT scale [6]. Long-lived particles are also a hallmark of split supersymmetry [7], where the gluino ($\tilde{g}$) decay is suppressed due to the large gluino-squark mass splitting, from which the theory gets its name. Of these possibilities, the Compact Muon Solenoid (CMS) experiment is most sensitive to models like split supersymmetry where production proceeds via the strong interaction resulting in relatively large cross sections at the Large Hadron Collider (LHC) [8–11]. Lifetimes of $\mathcal{O}$(100–1000) seconds are especially interesting in cosmology since such decays would affect the primordial light element abundances, and could resolve the present discrepancy between the measured ^{6}Li and ^{7}Li abundances and those predicted by conventional big-bang nucleosynthesis [12–14].

We have previously used this search to set limits on gluino production [15]; we now also place limits on production of scalar top. If long-lived gluinos (stops) are produced at the LHC, they will hadronise into $\tilde{g}g, \tilde{g}q\bar{q}, \tilde{g}qqq$ ($\tilde{t}q, \tilde{t}q\bar{q}$) states which are collectively known as "R-hadrons". In analogy with their mesonic and baryonic counterparts some of these bound states will be charged whilst others will be neutral. Those which are charged will lose energy via ionization as they traverse the detectors. For low-β R-hadrons, this energy loss is sufficient to bring a significant fraction of the produced particles to rest inside the detector volume [16]. These "stopped" R-hadrons could decay seconds, days, or weeks later. These decays would be out-of-time with respect to LHC collisions and may well occur at times when there are no collisions (e.g. beam gaps) or when there is no beam in the LHC machine (e.g. interfill period). The observation of such decays, in what should be a quiet detector save for the occasional cosmic ray, would be an unambiguous discovery of new physics. Searches for stopped particle decay have previously been performed at the Tevatron [17]. This search is complementary to methods that search for heavy stable charged particles by tracking their passage through the detector, using energy loss and timing information [18, 19].

The central feature of the Compact Muon Solenoid (CMS) apparatus is a superconducting solenoid, of 6 m internal diameter, providing a field of 3.8 T. Within the field volume are the silicon pixel and strip tracker, the crystal electromagnetic calorimeter (ECAL) and the brass/scintillator hadron calorimeter (HCAL). Muons are measured in gas-ionization detectors embedded in the steel return yoke. In addition to the barrel and endcap detectors, CMS has extensive forward calorimetry. In the region $|\eta| < 1.74$, the HCAL cells have widths of 0.087 in pseudorapidity and 0.087 rad in azimuth (ϕ). In the (η, ϕ) plane, and for $|\eta| < 1.48$, the HCAL cells map on to 5×5 ECAL crystals arrays to form calorimeter towers projecting radially outwards from close to the nominal interaction point. At larger values of $|\eta|$, the size of the towers increases and the matching ECAL arrays contain fewer crystals. Within each tower, the energy deposits in ECAL and HCAL cells are summed to define the calorimeter tower energies, subsequently used to provide the energies and directions of hadronic jets. A much more detailed description of CMS can be found elsewhere [20].

This Physics Analysis Summary describes a search for stopped particles in data recorded by CMS during April-July 2011. The analysis is essentially identical to that described in [15, 21], apart from minor changes detailed below.

2 Datasets

The search is performed in data recorded between April and July 2011. During this period the LHC instantaneous luminosity was increased to over 10^{33} cm^{-2}s^{-1}, largely by increasing the number of bunches injected for each fill. The radio frequency structure of LHC is such that proton bunches can collide every 25 ns. This interval defines the natural 40 MHz clock used to digitize signal from collisions. In the following each clock period is referred to as a "bunch-crossing", or BX. Since we search in gaps between colliding bunches, this has an effect on the amount of time that can be used for the search. This is summarised in Table 1, which gives the fraction of the orbit, f_{live}, that can be used for the search, for each filling scheme in the period analysed. This figure includes the effect of a 5 BX veto around each collision or unpaired bunch (as described later in Section 4), and a 35 BX period at the end of the abort gap that is used for calibration triggers. The total livetime in which the analysis is sensitive to decays of stopped particles, after accounting for these effects, is 168 hours.

We use the 2010 data as a control sample. This data is divided into two parts, 2010A and 2010B. In 2010A, 3.6 pb^{-1} were delivered to CMS during analysed luminosity sections, at a maximum instantaneous luminosity of 10^{28} cm^{-2}s^{-1}. The total livetime, in this dataset is 323 hours. In 2010B, 36 pb^{-1} were delivered in the analysed luminosity sections at a maximum instantaneous luminosity of 10^{32} cm^{-2}s^{-1}, with a total livetime of 97 hours.

Table 1: Summary of LHC filling schemes used for the search sample, showing the total number of bunches per beam, the total number of collisions per orbit at LHC P5, and the fraction of time available for the search, f_{live}. (In some cases a range of values is given for f_{live}. These result from multiple injection schemes that have the same number of total bunches, but different arrangements of bunches around the orbit.)

$N_{bunches}$	$N_{collision}$ (in CMS)	f_{live}
228	214	85%
336	322	78-79%
480	424	68%
624	598	61%
768	700	50-51%
912	874	44%
1092	1042	33%
1104	1042	32%
1236	1180	25%

3 Signal Simulation

The method used for simulating the atypical signal of a decaying stopped particle has not changed since [21]. We factorize the simulation into 3 phases. In Phase 1, we generate events at $\sqrt{s} = 7$ TeV using PYTHIA [22] to simulate the production of an HSCP and the subsequent hadronisation into an R-hadron. In the case of the gluino, the dominant leading order production processes are $q\bar{q} \to \tilde{g}\tilde{g}$ and $gg \to \tilde{g}\tilde{g}$, and in the case of the stop they are $q\bar{q} \to \tilde{t}\tilde{t}$ and $gg \to \tilde{t}\tilde{t}$. We scan gluino masses from $m_{\tilde{g}} = 300 - 900$ GeV/c^2, and stop masses from $m_{\tilde{g}} = 300 - 600$ GeV/c^2, ranges over which the theoretical production cross-section is sufficient that it can be probed with early LHC data. GEANT4 [23] is used to simulate the interaction of these R-hadrons with the CMS detector. To accomplish this, GEANT4 employs the so-called

"cloud model" for the interaction of stable heavy hadrons with matter [24, 25]. Eventually, the R-hadron either stops in the material of the detector, or exits it. In the former case the coordinates of the stopping point and the flavour of the R-hadron are recorded. R-hadrons that stop in CMS are typically produced with $\beta < 0.4$.

Figure 1 presents the stopping probability as a function of HSCP mass, obtained from the Phase 1 simulation. Nuclear interactions (NI) which depend on the cloud model introduce an uncertainty in the stopping probability. We therefore present the stopping probability from electromagnetic interactions (EM) alone, as well as that obtained from the combined effects of EM+NI. Some models [26] predict the lightest R-baryon ($\tilde{g}qqq$) state to be neutral, thus other R-baryons should quickly fall to this neutral state, and therefore escape the detector. In such models, only R-mesons ($\tilde{g}q\bar{q}$) will stop.

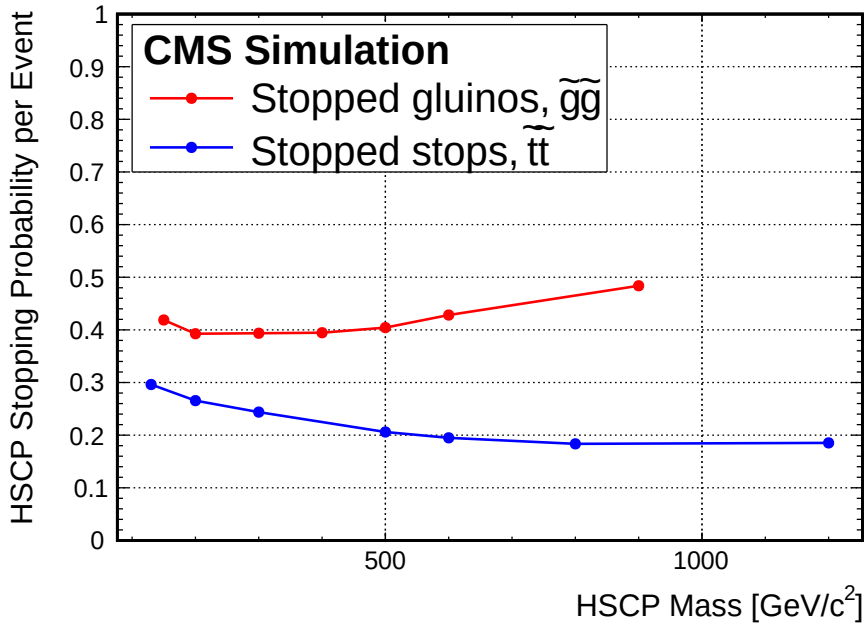

Figure 1: Probability for one of a pair of produced HSCPs to stop anywhere inside the CMS detector as a function of HSCP mass, at $\sqrt{s} = 7$ TeV.

In Phase 2, we simulate the decay of the stopped R-hadron. Implicit in our factorisation approach is the assumption that this decay takes place at a time that is much greater than the time required to stop the R-hadron. Thus we use PYTHIA to produce an R-hadron (with its flavour record from Phase 1) at rest at $(0, 0, 0)$. Subsequently, we translate the R-hadron from this nominal vertex position to a randomly chosen stopping location determined in Phase 1 and decay it instantaneously.

The kinematics of a R-hadron decay is dominated by the properties of the gluino, or stop, and neutralino - the spectator quarks do not play a significant role. These spectator quarks cannot be ignored, however, as they participate in hadronisation of the produced gluon or quarks. We developed and implemented a customised decay table to correctly describe these decays where a colour-neutral R-baryon decays into a coloured gluino, quark, and diquark with appropriate colour structure. In the analysis presented here, we assume BR($\tilde{g} \to g\tilde{\chi}_1^0$) = 100% and BR($\tilde{t} \to t\tilde{\chi}_1^0$) = 100%. Finally, PYTHIA hadronises the decay products, and parton-showering proceeds as usual. These fully simulated stopped gluino events are passed on to trigger emulation, then to default reconstruction, and are finally analysed as normal Monte Carlo data. With Phase 2

of the simulation we are thus able to estimate trigger and reconstruction efficiencies for any set of online and offline cuts.

Phase 3 of our simulation uses a toy Monte Carlo to determine how often a stopped HSCP decay will occur during a beam gap. The record of luminosity delivered by the LHC is taken from the CMS luminosity monitoring system [27]. This is used to randomly generate produced particles with the correct distribution in time. Next, the simulation determines when these particles decay. A random lifetime is then drawn from an exponential distribution with time constant equal to the proper lifetime of the HSCP, τ. In this way, we produce the distribution of particle decay times. By comparing with the LHC bunch structure, we calculate the fraction of observable events, and hence an effective integrated luminosity, for a given lifetime hypothesis.

The simulation performs similar steps to estimate the expected background. For this we use the rate of instrumental noise and cosmic-ray events, as measured during early 2010 collision data, described in Section 4. The background rate is multiplied by the trigger live-time and the resultant events are randomly assigned BXs and orbit numbers in either the collision or beam-gap periods.

4 Event Selection

We run a dedicated trigger to search for decays of particles at times when there are no collisions. Information from the beam position and timing (BPTX) monitors are used to flag beam gaps. The BPTX monitors are positioned 175 m around the LHC ring either side of the CMS interaction region, and produce a signal when an LHC bunch passes the monitor. The coincidence of signals from both BPTX indicates bunches passing in both directions, and hence the possibility for a pp collision.

For the stopped HSCP search, we require a jet trigger together with the condition that a signal from neither up or downstream BPTX occurred, ensuring that the trigger will not fire on jets produced from pp collisions, or beam-gas interactions from unpaired bunches. This veto is applied at the trigger level in a window of ± 1 BX around the triggered event. For the jet condition, we require a 32 GeV E_T threshold at the hardware trigger level (L1), and a 50 GeV energy threshold at the software trigger level (HLT). At both L1 and HLT, we require the pseudorapidity of the jet, $|\eta_{jet}|$, to be less than 3.0. Finally, at the trigger level, we also veto any event that is accompanied by a L1 endcap muon beam halo trigger, again within a ± 1 BX window.

We have used the simulation described in the previous sections to investigate the experimental signature of our atypical signal. Based on these studies, we have devised both topological and timing cuts which greatly reduce the instrumental and cosmic backgrounds while retaining good signal efficiency. These cuts are detailed in the rest of this section. As a benchmark for signal efficiency, we quote figures for the $m_{\tilde{g}} = 500\,\mathrm{GeV}/c^2$, $M_{\tilde{\chi}_1^0} = 400\,\mathrm{GeV}/c^2$ Monte Carlo sample.

Imperfections in the detector synchronisation may result in triggers from collisions events that are 1 or more BX early or late with respect to the collision itself. We therefore reject any event falling within $\pm$ 2 BX of any passage of beam. We also veto any event containing a reconstructed vertex. The most significant source of beam-related background comes from beam halo events. We therefore veto any event identified by the standard CMS loose beam halo algorithm, based on the endcap muon system. A small fraction of cosmic rays traversing CMS deposit significant energy in the calorimeters. To remove such background, we veto events which contain 1 or more muons.

Once beam related backgrounds and cosmic rays are removed, the remaining source of background is detector noise. We apply standard CMS calorimeter cleaning and noise rejection cuts [28–30]. In addition, we also make the following cuts on the shape and magnitude of hadronic calorimeter (HCAL) energy deposits in order to discriminate against HCAL instrumental noise.

Firstly, we restrict our search to jets in the central HCAL only. Since most HSCP bound states are produced centrally due to their high mass, the endcaps and forward calorimeters (which tend to be noisier) do not contribute much to the signal rate. Hence we require that the most energetic jet in the event has $|\eta_{jet}| < 1.$. This cut has been tightened from the value of 1.3 used in the 2010 analysis, to improve rejection of beam halo events, which peak above this value.

To reject fluctuations over the jet threshold and energy deposits from minimum ionising particles we make a cut on the reconstructed jet energy at 70 GeV. To remove events where a single HCAL channel has fired, we veto events where the number of towers containing 90% of the energy (n_{90}) is 3 or less. We also veto wide jets characteristic of noise by removing events where the number of towers containing 60% of the leading jet energy (n_{60}) is less than 6. Noise may be distinguished from physical signals using the mapping of towers to their readout electronics. The 18 channels readout by a single hybrid photodiode all correspond to the same ϕ value, hence we order the HCAL towers by energy, and count the number of leading towers at the same ϕ. If this value, n_{iphi}, is greater than 5, we reject the event. Finally, we compute the largest fraction of jet energy contained within a single strip of towers at constant phi, and we require that this value be less than 95%.

The HCAL electronics have a well-defined time response to charge deposits generated by showering particles. This pulse shape can be used to distinguish deposits from real physics processes from pulses generated by electronics noise, which may not have a physics-like time profile. A physical pulse has some notable properties which can be used to distinguish it from the noise pulses. There is a clear trigger-peak, (BX_{Peak}), significant energy in one bunch crossing before the peak (BX_{Peak-1}) and an exponential decay for several BX's following the peak. We have developed several powerful though correlated cuts that distinguish physical pulses from noise. We use the ratios $R_1 = BX_{peak+1}/BX_{peak}$ and $R_2 = BX_{peak+2}/BX_{peak+1}$ to characterise the exponential decay, requiring $0.15 < R_1$ and $0.1 < R_2 < 0.8$. Ten time samples (each 25 ns in length) are read out by the HCAL, allowing us to reject noise events based on the presence of energy in earliest or latest BX's, since the "physics pulse shape" covers only 4 time samples. We cut events with more than 30% of the energy of the pulse outside of the central four BX's. Deposits from physical particles tend to have a large fraction of the pulse energy in the peak BX. Noise can have a variety of pulse shapes from having energy spread across many BX's to having almost all energy localised in one BX. We make a cut on the peak fraction of $0.3 < BX_{Peak}$ / Total Energy < 0.7.

The background rate and signal efficiency after each cut is summarised in Table 2. Table 3 shows the efficiencies for Monte Carlo samples with a range of $m_{\tilde{g}}$ and $M_{\tilde{\chi}_1^0}$. After all cuts, the efficiency for a gluino signal (with $m_{\tilde{g}} = 500$ GeV/c^2 and $M_{\tilde{\chi}_1^0} = 400$ GeV/c^2) estimated from the simulation, is 13.3% of all stopped particles, or 42.0% of all event passing the HLT.

The background to the counting experiment comprises components of instrumental noise, unidentified cosmic rays, and unidentified beam backgrounds, principally beam halo. We estimate the component due to instrumental noise and unidentified cosmic rays from the final rate in the 2010A dataset, which was taken during fills with very low instantaneous luminosity, measured to be $5.2 \pm 2.1(\text{stat}) \times 10^{-6}$ Hz. To estimate the component due to unidentified beam

backgrounds, we take the difference between the rate measured in 2010B and 2010A, which is found to be $1.2 \pm 0.7(\text{stat}) \times 10^{-5}$ Hz. Finally, we estimate the background in the 2011 search dataset by taking the sum of these components, which is identical to the final rate measured in the 2010B dataset; $1.7 \pm 0.7(\text{stat}) \times 10^{-5}$ Hz.

Table 2: Background rate determined from the 2010B dataset, and expected signal efficiency for the $m_{\tilde{g}} = 500$ GeV/c^2 and $M_{\tilde{\chi}_1^0} = 400$ GeV/c^2 Monte Carlo sample, after each online and offline cut. Note, the signal efficiency is quoted with respect to the fraction of events in which one of the two produced gluinos stops anywhere in the CMS detector (including uninstrumented regions).

Selection Criteria	Background Rate (Hz)	Signal Efficiency %
trigger	21.5 ± 0.008	31.3
BX veto	8.61 ± 0.005	31.3
Vertex veto	8.61 ± 0.005	31.3
Halo veto	8.28 ± 0.0049	31.2
Cosmic veto	8.19 ± 0.0049	26.8
Noise veto	6.79 ± 0.0044	26.2
$E_{jet} > 70$ GeV	$2.63 \pm 0.028 \times 10^{-2}$	14.6
$n60_{jet} < 6$	$2.63 \pm 0.028 \times 10^{-2}$	14.5
$n90_{jet} > 3$	$2.33 \pm 0.082 \times 10^{-3}$	13.3
$nTowiPhi < 5$	$4.0 \pm 1.1 \times 10^{-5}$	13.3
$E_{iphi}/E_{jet} < 0.95$	$2.3 \pm 2.3 \times 10^{-5}$	13.3
$R_1 > 0.15$	$2.3 \pm 2.3 \times 10^{-5}$	13.4
$0.1 < R_2 < 0.8$	$2.3 \pm 2.3 \times 10^{-5}$	13.4
$0.3 < R_{peak} < 0.7$	$1.7 \pm 0.7 \times 10^{-5}$	13.3
$R_{outer} < 0.3$	$1.7 \pm 0.7 \times 10^{-5}$	13.3

Table 3: Selection efficiency as a function of m_{HSCP} and $M_{\tilde{\chi}_1^0}$. Efficiency is quoted here with respect to the fraction of events in which one of the two produced gluinos stops anywhere in the *whole* CMS detector.

$m_{\tilde{g}}$ (GeV/c^2)	$M_{\tilde{\chi}}$ (GeV/c^2)	efficiency (% of stopped)
300	200	12.0%
400	300	13.2%
500	400	13.3%
600	500	13.3%
900	800	13.1%
$m_{\tilde{t}}$ (GeV/c^2)	$M_{\tilde{\chi}}$ (GeV/c^2)	efficiency (% of stopped)
300	100	12.1%

5 Sources of Systematic Uncertainty

The generic search for stopped particles described in this note is, by design, minimally exposed to systematic uncertainties. As described in Section 1, the background estimate is taken from a control sample of data taken in late 2010. The dominant uncertainty on the background estimate is the statistical uncertainty in this sample, 40%. There is a small systematic uncertainty

due to the jet energy scale (JES). For a JES uncertainty of $\pm 10\%$, we estimate a 7% effect on the cross-section limit. The systematic uncertainty due to trigger efficiency is negligible since the data analysed are well above the turn-on region. Similarly, the systematic uncertainty due to reconstruction efficiency is negligible since we restrict our search to $m_{\tilde{g}} - M_{\tilde{\chi}_1^0} > 100$ GeV/c^2, for gluino, and $m_{\tilde{t}} - M_{\tilde{\chi}_1^0} > 200$ GeV/c^2 for stop. Finally, there is a 6% uncertainty on the luminosity.

Limits on a particular model (e.g. gluinos in split supersymmetry) introduce more substantial systematic uncertainties, since the signal yield is sensitive to the stopping probability. The GEANT4 simulation used to derive the stopping efficiency described in Section 3 implements models for both electromagnetic (EM) and nuclear interaction (NI) energy loss mechanisms. Whereas the EM model is well understood, the R-hadron "cloud model" used for NI has never been tested and is based on speculative physics extrapolated from low-energy QCD. Moreover, there are alternative models [26] in which R-hadrons preferentially become neutral after NI. While both the neutral R-hadron and EM only models are likely pessimistic scenarios, in Figure 4 we present limits employing both the cloud and EM only models. The range spanned by the two curves represents the uncertainty on the limit due to the stopping model.

6 Search Results

After the selection criteria described in the preceding paragraphs are applied, we perform a counting experiment and a time-profile analysis on the remaining data. The method is unchanged since [15, 21]. For the counting experiment, we consider HSCP lifetime hypotheses from 75 ns to 10^6 seconds. For lifetime hypotheses shorter than one LHC orbit (89 μs), we search within a time window following each collision, equal to $1.3 \times \tau$, for optimal sensitivity to each hypothesized lifetime τ. In addition to the lifetimes required to map the general features of the exclusion limit, we include two lifetimes for each observed event: the largest lifetime hypothesis for which the event lies outside the time window, and the smallest lifetime hypothesis for which the event is contained within the time window. For lifetime hypotheses longer than one LHC fill, we do not consider the possibility that any observed events may have come from HSCPs produced in a previous fill.

In the search sample, we do not observe a significant excess above expected background for any lifetime hypothesis. The results of this counting experiment for selected lifetime hypotheses are presented in Table 4, along with the effective luminosity, calculated using the toy MC described in Section 3. In the absence of any discernible signal, we proceed to set 95% confidence level (C.L.) limits over 13 orders of magnitude in HSCP lifetime using the standard CMS Exotica Bayesian calculator implemented in ROOSTATS. The resulting model-independent limit on particle production cross-section $\times$ branching ratio $\times$ stopping probability is shown in Figure 2. The limit is presented for gluino with $m_{\tilde{g}} = 500$ GeV/c^2 and $M_{\tilde{\chi}_1^0} = 400$ GeV/c^2, and stop with $m_{\tilde{t}} = 300$ GeV/c^2 and $M_{\tilde{\chi}_1^0} = 100$ GeV/c^2.

We also perform a time-profile analysis. Whereas, for short lifetimes, a signal from a stopped HSCP decay is correlated in time with the collisions, backgrounds are flat in time. Since the signal and background have very different time profiles, it is possible to extract both their contributions by analyzing the distribution of the observed events in time. We assume all colliding bunches in an orbit have equal individual instantaneous luminosity. We build a probability density function (PDF) for the HSCP decay signal as a function of BX, for a given HSCP lifetime hypothesis and the actual times of LHC collisions as recorded in our data. A set of signal PDFs used in the time-profile analysis, for a 1 μs lifetime hypothesis, are shown in Figure 3,

with observed events overlaid. For lifetimes much longer than the length of the gaps between bunch crossings, the signal PDF becomes flat and background-like, and the sensitivity of the method naturally degrades. We perform the analysis for lifetimes up to 0.7 ms, which is sufficiently long that this degradation can be observed.

Table 4: Results of counting experiments for selected τ, including the effective integrated luminosity, L_{eff}, calculated with toy MC.

Lifetime	$L_{eff}(pb^{-1})$	Expected Bg	Observed
75 ns	4.3	0.11 ± 0.05	0
100 ns	12.5	0.35 ± 0.14	0
1 μs	139	3.3 ± 1.3	4
10 μs	352	10.1 ± 4.1	9
30 μs - 10^3 s	360	10.4 ± 4.2	10
10^4 s	268	10.4 ± 4.2	10
10^5 s	65	10.4 ± 4.2	10
10^6 s	7.5	10.4 ± 4.2	10

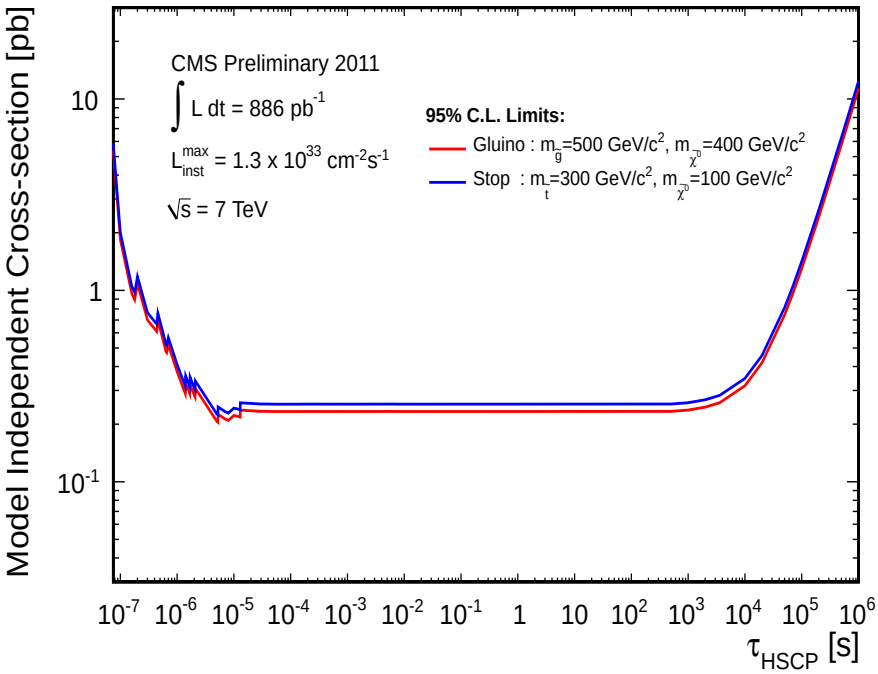

Figure 2: 95% C.L. limits on HSCP pair production cross-section times the probability of either HSCP to stop, as a function of HSCP lifetime.

Including the stopping probability obtained from simulation (Section 3), we then place limits on the particle production cross-section. Figures 4 and 5 show the observed 95% C.L. limits on gluino and stop pair production cross-sections, for different models of R-hadron interactions, as a function of particle lifetime assuming 100% branching ratio, and fixed visible energy of $m_{HSCP} - M_{\tilde{\chi}_1^0} > 100$ GeV/c^2. The stopping probability used to construct these limits assume $m_{\tilde{g}} = 500$ GeV/c^2 and $m_{\tilde{t}} = 300$ GeV/c^2; the variation of the limit with HSCP mass may be inferred from Figures 6 and 7.

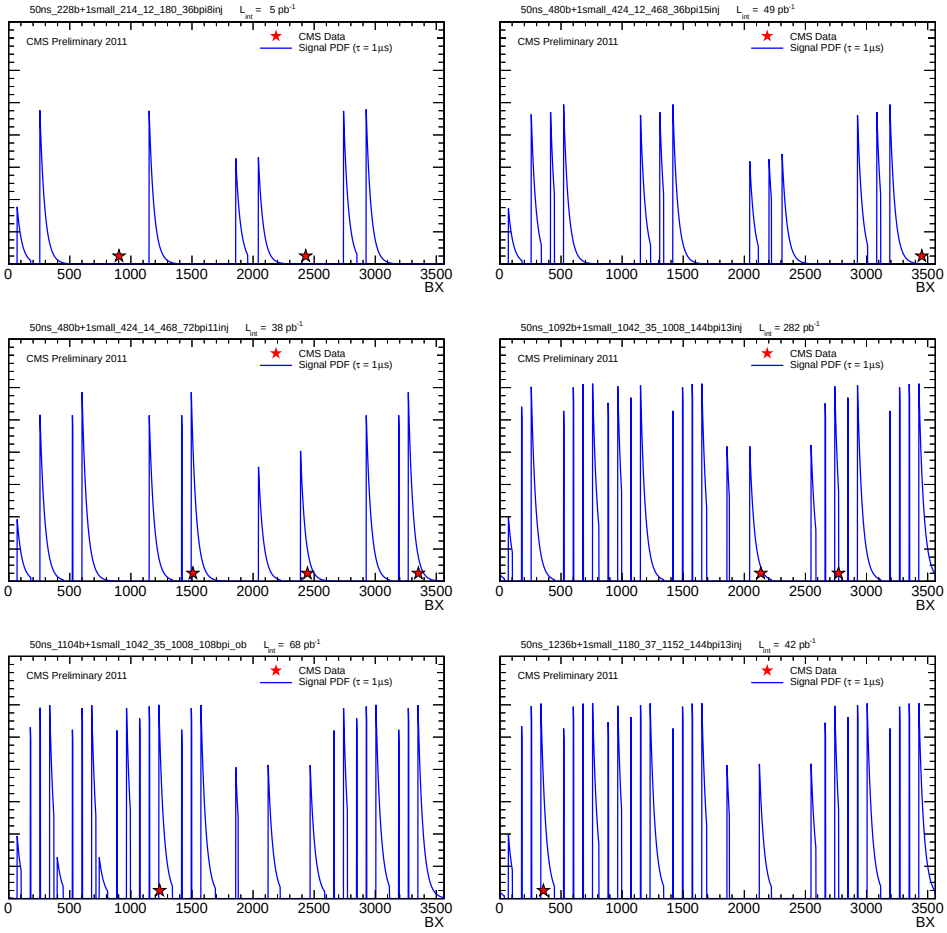

Figure 3: In orbit position of observed events, overlaid on the decay profile for a 1 μs lifetime hypothesis produced during the same fills. The vertical axis uses arbitrary units. The integrated luminosity figures give the amount analysed for each filling scheme. (Note that the total is not 886 pb^{-1} since filling schemes in which no events were observed are not shown).

Finally, Figures 6 and 7 show the limit on production cross-section as a function of stopped particle mass. Assuming the theoretical production cross-section for the HSCP [31], we are able to exclude $m_{\tilde{g}} < 601$ GeV/c^2, and $m_{\tilde{t}} < 337$ GeV/c^2 at 95% C.L. Figure 8 shows observed limits for gluino and stop on the same plot.

7 Conclusions

In this Physics Analysis Summary we have presented updated results of a search for long-lived particles which have stopped in the Compact Muon Solenoid detector after being produced in 7 TeV pp collisions from CERN's Large Hadron Collider. We looked for the subsequent decay of these particles during time intervals where there were no pp collisions in the Compact Muon Solenoid experiment. In particular, we searched for decays during gaps between crossings in the Large Hadron Collider beam structure, recorded with dedicated calorimeter triggers. In a dataset with a peak instantaneous luminosity of 1.3×10^{33} cm^{-2}s^{-1}, an integrated luminosity of up to 886 pb^{-1} lifetime, and a search interval corresponding to 168 hours of trigger live time, no significant excess above background was observed. In the absence of a signal, we set a limit at 95% C.L. on HSCP pair production over 13 orders of magnitude of HSCP lifetime. For a mass

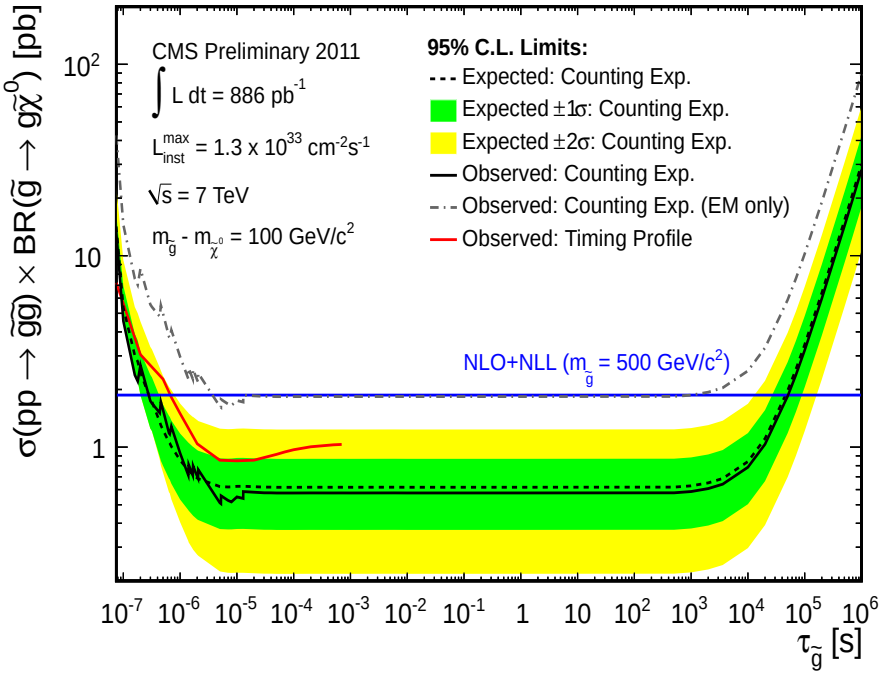

Figure 4: Expected and observed 95% C.L. limits on gluino pair production cross-section using the "cloud model" of R-hadron interactions as a function of gluino lifetime from both counting experiment and the time profile analysis. Errors include statistical plus systematic uncertainties. Observed 95% C.L. limits on the gluino cross-section for alternative R-hadron interaction models are also presented. The NLO+NLL calculation is from [31]. The structure observed between 10^{-6} s and 10^{-4} s is due to the number of observed events incrementing when crossing boundaries between lifetime bins.

difference $m_{\tilde{g}} - M_{\tilde{\chi}_1^0} > 100$ GeV/c^2, assuming BR($\tilde{g} \to g\tilde{\chi}_1^0$) = 100%, we are able to exclude a gluino with lifetimes from 10 μs to 1000 s and $m_{\tilde{g}} < 601$ GeV/c^2. Under similar assumptions, $m_{\tilde{t}} - M_{\tilde{\chi}_1^0} > 200$ GeV/c^2, and BR($\tilde{t} \to t\tilde{\chi}_1^0$) = 100%, we are able to exclude a stop with lifetimes from 10 μs to 1000 s and $m_{\tilde{t}} < 337$ GeV/c^2. This result is consistent with the complementary exclusion provided by the direct HSCP search [19].

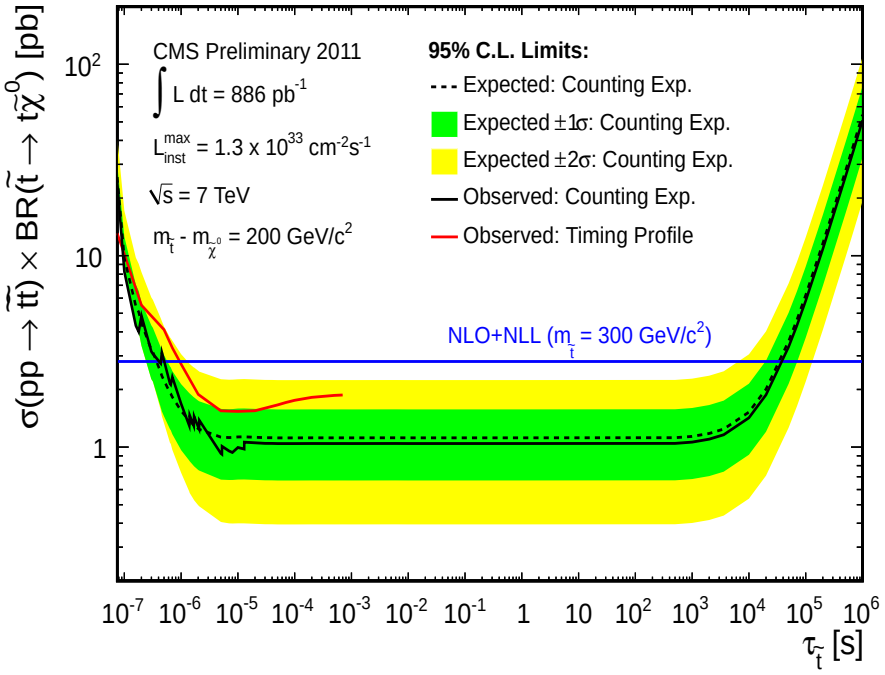

Figure 5: Expected and observed 95% C.L. limits on stop pair production cross-section using the "cloud model" of R-hadron interactions, as a function of stop lifetime from both counting experiment and the time profile analysis. Errors include statistical plus systematic uncertainties. The NLO+NLL calculation is from [31]. The structure observed between 10^{-6} s and 10^{-4} s is due to the number of observed events incrementing when crossing boundaries between lifetime bins.

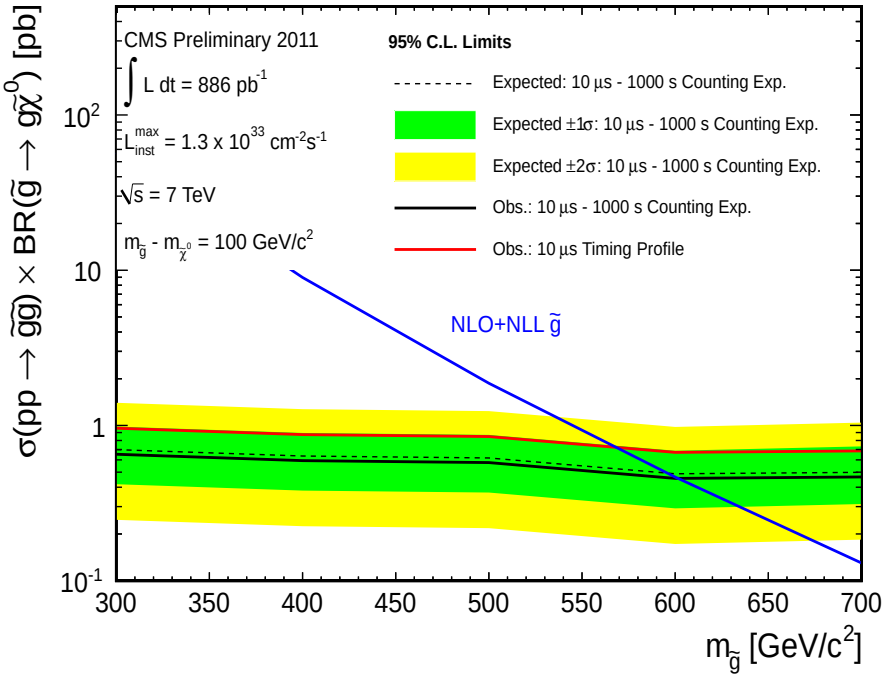

Figure 6: 95% C.L. limits on gluino pair production cross-section as a function of $m_{\tilde{g}}$ assuming the "cloud model" of R-hadron interactions. The $m_g - M_{\tilde{\chi}_1^0}$ mass difference is maintained at 100 GeV/c^2. The NLO+NLL calculation is from [31].

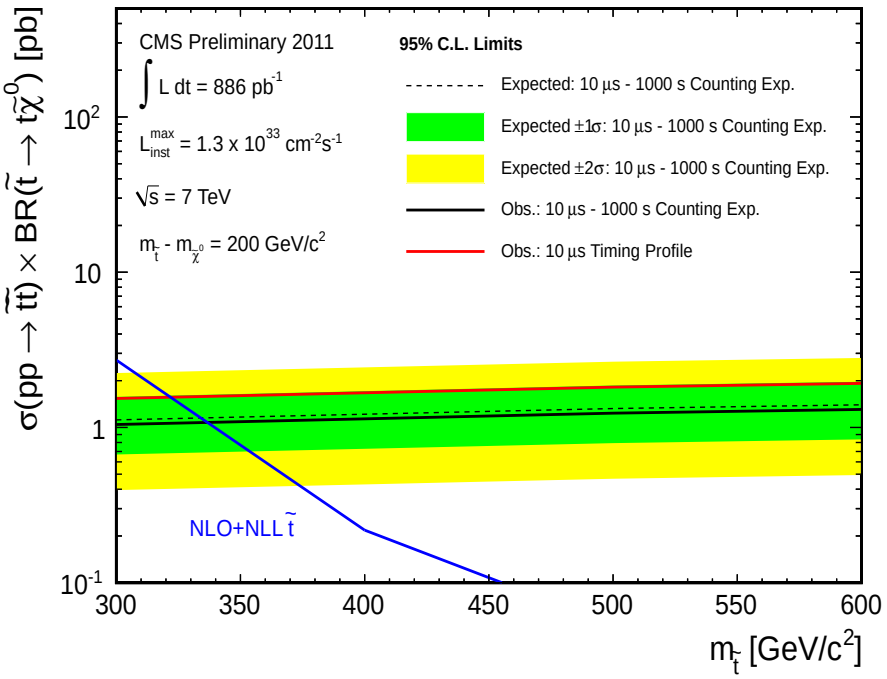

Figure 7: 95% C.L. limits on stop pair production cross-section as a function of $m_{\tilde{t}}$ assuming the "cloud model" of R-hadron interactions. The $m_t - M_{\tilde{\chi}_1^0}$ mass difference is maintained at 200 GeV/c^2. The NLO+NLL calculation is from [31].

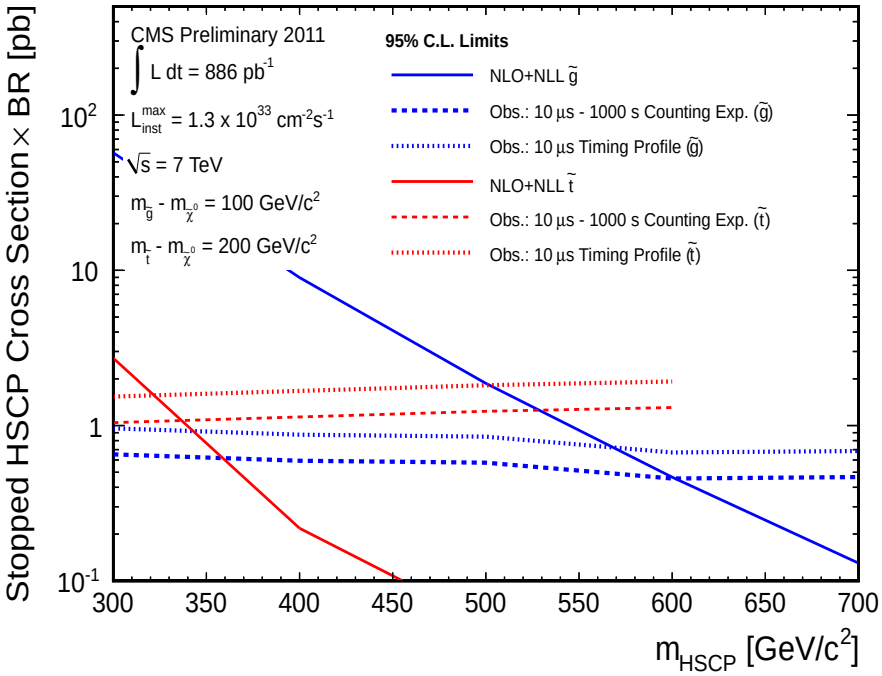

Figure 8: 95% C.L. limits on gluino and stop pair production cross-sections as a function of HSCP mass. The "cloud model" of R-hadron interactions is assumed. For gluino, the $m_g - M_{\tilde{\chi}_1^0}$ mass difference is maintained at 100 GeV/c^2, and for stop, $m_t - M_{\tilde{\chi}_1^0}$ is maintained at 200 GeV/c^2. The NLO+NLL calculation is from [31].

References

[1] M. Fairbairn et al., "Stable massive particles at colliders", *Phys. Rept.* **438** (2007) 1–63, arXiv:hep-ph/0611040. doi:10.1016/j.physrep.2006.10.002.

[2] S. Dimopoulos, M. Dine, S. Raby et al., "Experimental Signatures of Low Energy Gauge Mediated Supersymmetry Breaking", *Phys. Rev. Lett.* **76** (1996) 3494–3497, arXiv:hep-ph/9601367. doi:10.1103/PhysRevLett.76.3494.

[3] H. Baer, K.-m. Cheung, and J. F. Gunion, "A Heavy gluino as the lightest supersymmetric particle", *Phys. Rev.* **D59** (1999) 075002, arXiv:hep-ph/9806361. doi:10.1103/PhysRevD.59.075002.

[4] T. Jittoh, J. Sato, T. Shimomura et al., "Long life stau", *Phys. Rev.* **D73** (2006) 055009, arXiv:hep-ph/0512197. doi:10.1103/PhysRevD.73.055009.

[5] M. J. Strassler and K. M. Zurek, "Echoes of a hidden valley at hadron colliders", *Phys. Lett.* **B651** (2007) 374–379, arXiv:hep-ph/0604261. doi:10.1016/j.physletb.2007.06.055.

[6] A. Arvanitaki et al., "Astrophysical Probes of Unification", *Phys. Rev.* **D79** (2009) 105022, arXiv:0812.2075. doi:10.1103/PhysRevD.79.105022.

[7] N. Arkani-Hamed and S. Dimopoulos, "Supersymmetric unification without low energy supersymmetry and signatures for fine-tuning at the LHC", *JHEP* **06** (2005) 073, arXiv:hep-th/0405159.

[8] S. Dawson, E. Eichten, and C. Quigg, "Search for Supersymmetric Particles in Hadron - Hadron Collisions", *Phys. Rev.* **D31** (1985) 1581. doi:10.1103/PhysRevD.31.1581.

[9] W. Beenakker, R. Hopker, M. Spira et al., "Squark and gluino production at hadron colliders", *Nucl. Phys.* **B492** (1997) 51–103, arXiv:hep-ph/9610490. doi:10.1016/S0550-3213(97)00084-9.

[10] T. Plehn, D. Rainwater, and P. Z. Skands, "Squark and gluino production with jets", *Phys. Lett.* **B645** (2007) 217–221, arXiv:hep-ph/0510144. doi:10.1016/j.physletb.2006.12.009.

[11] W. Beenakker et al., "Soft-gluon resummation for squark and gluino hadroproduction", *JHEP* **12** (2009) 041, arXiv:0909.4418. doi:10.1088/1126-6708/2009/12/041.

[12] K. Jedamzik, "Did something decay, evaporate, or annihilate during big bang nucleosynthesis?", *Phys. Rev.* **D70** (2004) 063524, arXiv:astro-ph/0402344. doi:10.1103/PhysRevD.70.063524.

[13] K. Jedamzik et al., "Solving the cosmic lithium problems with gravitino dark matter in the CMSSM", *JCAP* **0607** (2006) 007, arXiv:hep-ph/0512044. doi:10.1088/1475-7516/2006/07/007.

[14] S. Bailly, K. Jedamzik, and G. Moultaka, "Gravitino Dark Matter and the Cosmic Lithium Abundances", *Phys. Rev.* **D80** (2009) 063509, arXiv:0812.0788. doi:10.1103/PhysRevD.80.063509.

[15] CMS Collaboration, "Search for Stopped Gluinos in pp collisions at sqrt s = 7 TeV", *Phys. Rev. Lett.* **106** (2011) 011801, arXiv:1011.5861. doi:10.1103/PhysRevLett.106.011801.

[16] A. Arvanitaki, S. Dimopoulos, A. Pierce et al., "Stopping gluinos", *Phys. Rev.* **D76** (2007) 055007, arXiv:hep-ph/0506242. doi:10.1103/PhysRevD.76.055007.

[17] D0 Collaboration, "Search for stopped gluinos from $p\bar{p}$ collisions at $\sqrt{s}$ = 1.96-TeV", *Phys. Rev. Lett.* **99** (2007) 131801, arXiv:0705.0306. doi:10.1103/PhysRevLett.99.131801.

[18] ATLAS Collaboration Collaboration, "Search for Heavy Long-Lived Charged Particles with the ATLAS detector in pp collisions at sqrt(s) = 7 TeV", arXiv:1106.4495. * Temporary entry *.

[19] CMS Collaboration, "Search for Heavy Stable Charged Particles in pp collisions at $\sqrt{s} = 7$ TeV", *CMS Physics Analysis Summary* **CMS-PAS-EXO-11-022** (2011).

[20] CMS Collaboration, "The CMS experiment at the CERN LHC", *JINST* **0803** (2008) S08004. doi:10.1088/1748-0221/3/08/S08004.

[21] CMS Collaboration, "Search for Stopped Gluinos in pp collisions at $\sqrt{s}$ = 7 TeV", *CMS Physics Analysis Summary* **CMS-PAS-EXO-10-003** (2010).

[22] T. Sjostrand, S. Mrenna, and P. Z. Skands, "PYTHIA 6.4 Physics and Manual", *JHEP* **05** (2006) 026, arXiv:hep-ph/0603175.

[23] GEANT4 Collaboration, "GEANT4: A simulation toolkit", *Nucl. Instrum. Meth.* **A506** (2003) 250–303. doi:10.1016/S0168-9002(03)01368-8.

[24] A. C. Kraan, "Interactions of heavy stable hadronizing particles", *Eur. Phys. J.* **C37** (2004) 91–104, arXiv:hep-ex/0404001. doi:10.1140/epjc/s2004-01997-7.

[25] R. Mackeprang and A. Rizzi, "Interactions of coloured heavy stable particles in matter", *Eur. Phys. J.* **C50** (2007) 353–362, arXiv:hep-ph/0612161. doi:10.1140/epjc/s10052-007-0252-4.

[26] F. Buccella, G. R. Farrar, and A. Pugliese, "R Baryon masses", *Phys. Lett.* **B153** (1985) 311. doi:10.1016/0370-2693(85)90555-6.

[27] CMS Collaboration, "Measurement of CMS Luminosity", *CMS Physics Analysis Summary* **CMS-PAS-EWK-10-004** (2010).

[28] CMS Collaboration, "Identification and Filtering of Uncharacteristic Noise in the CMS Hadron Calorimeter", *JINST* **5** (2010) T03014, arXiv:0911.4881. doi:10.1088/1748-0221/5/03/T03014.

[29] CMS Collaboration, "HCAL Commissioning in Proton Collisions at $\sqrt{s} = 7$ TeV", *CMS Physics Analysis Summary* **CMS-PAS-JME-10-007** (2010).

[30] CMS Collaboration, "MET Performance in Minimum-Bias and Jet Events from Proton-Proton Collisions at $\sqrt{s} = 7$ TeV", *CMS Physics Analysis Summary* **CMS-PAS-JME-10-004** (2010).

[31] W. Beenakker et al., "Squark and gluino hadroproduction", arXiv:1105.1110.